Zn and N Co-doped TiO_2 Thin Films: Photocatalytic and Bactericidal Activity

Abdullah M Alotaibi[a,b], Premrudee Promdet[a], Gi Byoung Hwang[a], Jianwei Li[a], , Sean P. Nair[c], Sanjayan Sathasivam[a], Andreas Kafizas[d,e], Claire J. Carmalt[a] and Ivan P Parkin[a]*

*Corresponding author

[a]Materials Chemistry Centre, Department of Chemistry, University College London, 20 Gordon Street, London WC1H 0AJ, UK

[b]The National Centre for Building and Construction Technology, King Abdulaziz City for Science and Technology (KACST), Riyadh, 11442-6086, Saudi Arabia

[c]Department of Microbial Diseases, UCL Eastman Dental Institute, 256 Gray's Inn Road, London, WC1X 8LD

[d]Department of Chemistry, Imperial College London, South Kensington, London, SW7 2AZ, UK

[e]The Grantham Institute, Imperial College London, South Kensington, London, SW7 2AZ, UK

E-mail: i.p.parkin@ucl.ac.uk

Abstract

In this article, we explore a series of Zn and N co-doped TiO_2 thin films grown using chemical vapour deposition. Films were prepared with various concentrations of Zn (0.4 - 2.9 at.% Zn *vs* Ti), and their impact on superoxide formation, photocatalytic activity and bactericidal properties were determined. Superoxide ($O_2^{\bullet-}$) formation was assessed using a 2,3-bis(2-methoxy-4-nitro-5-sulfophenyl)-5-[(phenylamino)carbonyl]-2H-tetrazolium sodium salt (XTT) as an indicator, photocatalytic activity was determined from the degradation of stearic acid under UVA light and bactericidal activity was assessed using a Gram-negative bacterium *E. coli* under both UVA and fluorescent light (similar to what is found in a clinical environment). Compared with undoped TiO_2, the 1.0% Zn, N : TiO_2 thin film demonstrated a higher formal quantum efficiency in degrading stearic acid (2.5×10^{-5} *vs* $1.5x\ 10^{-5}$ molecules.photon^{-1}) and a higher bactericidal activity (> 3 log kill under UVA and fluorescent light conditions *vs* < 0.5 log kill under UVA and fluorescent light conditions). The enhanced efficiency of the films was correlated with increased charge carrier lifetime, supported by transient absorption spectroscopy (TAS) measurements.

Keywords: Photocatalysis, Antibacterial surfaces, CVD, TiO_2, Transient Absorption Spectroscopy

Introduction

Titanium dioxide (TiO_2) is a widely studied photocatalyst, due to its high activity in degrading a range of organic materials, chemical/biological stability and low cost.[1–4] Anatase, the most photoactive polymorph of TiO_2, has an indirect bandgap of 3.2 eV, and upon activation by UV light of sufficient energy, electrons are excited from the valence to the conduction band, leaving behind holes.[5] The photogenerated electrons and holes can diffuse to the surface of TiO_2 and react with e.g. O_2 and H_2O to produce reactive oxygen species (ROS) such as $^{\bullet}O_2^-$ and $^{\bullet}OH$. These ROS (as well as electrons and holes directly) can degrade organic contaminants and clean the surrounding environment - be that air or water.[6] Photoinduced ROS from TiO_2 are non-selective and thus are also destructive against bacteria, therefore giving TiO_2 antibacterial properties.[7–9] It has been shown that there is a direct correlation between generated ROS and bactericidal activity.[8] Hydroxyl radicals ($^{\bullet}OH$) radicals can damage DNA, nucleic acids and amino acids.[10] Whereas $^{\bullet}O_2^-$ can damage tissue and degrade the cell membrane. [11] Detection of ROS generated from metal oxides has been extensively investigated. The 2,3-bis(2-methoxy-4-nitro-5-sulfophenyl)-5-[(phenylamino)carbonyl]-2H-tetrazolium sodium salt (XTT), 3-(4,5-dimethyl-2-thiazol)-2,5-diphenyl-2H-tetrazolium bromide (MTT) and nitroblue tetrazolium (NBT) have been used to detect $^{\bullet}O_2^-$. XTT has been extensively used due to it being reduced to XTT formazan by $^{\bullet}O_2^-$. For instance, Chen and et al.[8] used XTT sodium salt to detect $^{\bullet}O_2^-$ anion radicals generated from nanoparticles of TiO_2 under UVA irradiation (365 nm). Wang and Zhao[12] also used XTT and NBT as probes for detecting $^{\bullet}O_2^-$ radicals generated in the presence of histidine under UV irradiation. And Zhao and Jafvert used XTT for detecting the generation of $^{\bullet}O_2^-$ from graphene oxide under UV irradiation.[13]

In an effort to improve the photocatalytic self-cleaning and antibacterial properties of TiO_2, extrinsic doping has been investigated.[1415] Reports on the doping of TiO_2 are plentiful, with nitrogen being the most popular dopant.[16–18] The primary motive for N doping has been to reduce the wide (3.0 - 3.2 eV) and only UV light ($\lambda < 380$ nm) active bandgap of TiO_2 to the visible range.[14] The reduction in the bandgap arises due to the formation of occupied N 2p states above the TiO_2 valence band maximum,

which form when N replaces O sites i.e. when substitutional doping occurs. Reduced bandgap N : TiO_2 allows the harvesting of a much larger portion of the solar spectrum (~40%) compared to the nominally undoped form (~5% of the solar spectrum), potentially allowing for a more efficient photocatalytic device.[14] However, in practice, this is often not so simple. One of the disadvantages of N doping is the localised nature of the N 2p orbitals, where holes generated upon visible light irradiation have reduced mobility compared to holes generated in the O 2p orbitals by UV irradiation, and thus do not reach the TiO_2 surface as readily to carry out redox reactions.[14,16,17] Furthermore, due to the smaller bandgap, visible light induced holes would have lower oxidation potential, in producing ROS for photocatalytic applications, therefore limiting performance.[19–22] A potentially more useful strategy to increase photocatalytic performance is *via* interstitial doping (N_i), whereby the N occupies the space between the Ti and O in the lattice. N_i results in occupied anti-bonding states above the valence band (along with bonding states within the valence band) but causes no reduction in the bandgap.[14] The presence of N_i has been shown to increase UV photocatalysis via the extension of carrier lifetimes.[21]

Similarly, zinc doping has also been shown to enhance the UV light activated photocatalytic performance of TiO_2 by facilitating the separation of carriers. This was found to be the case by Zhao et al. for Zn : TiO_2 nanoparticles and by Zhang et al. for DC sputtered films.[23,24] With respect to antibacterial properties, Zn as a dopant has an added benefit in that Zn ions are believed to be cytoxins to bacterial cells at levels above 10^{-7} mol L^{-1}.[25]

The use of both anionic (such as N_i) and cationic (such as Zn) co-dopants is adventitious in delivering electronic modifications for enhanced UV photocatalysis as these dopants do not compete for the same site in the TiO_2 lattice.[26,27]

In this paper, thin films of Zn and N co-doped TiO_2 were grown by aerosol-assisted chemical vapour deposition (AACVD); an ambient pressure scalable route to functional films.[25,28–30] In fact, CVD is the method of choice for the growth of self-cleaning TiO_2 coatings for architectural glass panels.[28] The effect of altering the Zn doping level (from 0.4 – 2.9 at.% Zn *vs* Ti) on the photocatalytic and bactericidal activity was investigated using a model pollutant (stearic acid) and Gram-negative bacteria (*Escherichia coli*) under UVA and fluorescent light irradiation. To explain

the observed activity trends, the photoinduced production of ROS was studied using the indicator, XXT sodium salt, and charge carrier lifetimes were probed using transient absorption spectroscopy (TAS).

Experimental

Thin film fabrication

Titanium butoxide (99.9%) and ethanol (99.8%) were purchased from Merck and Zinc-2-ethylhexanoate (99%) from Strem Chemicals, Inc.; they were used as received. Depositions were carried out on 150 × 45 × 4 mm SiO_2 barrier coated (50 nm thick layer) float-glass, supplied by Pilkington NSG. Prior to use, the glass substrates were thoroughly cleaned using acetone (99%), isopropanol (99.9%) and distilled water and dried in air. For the fabricating N : TiO_2, a precursor solution was made by dissolving titanium butoxide [$Ti(OCH_2CH_2CH_2CH_3)_4$, 0.5 g, 1.5 mmol] and *tert*-butylamine [($C_4H_{11}N$ 99.5%), 3.6 mL] in ethanol (25 ml) in a glass bubbler. For the fabricating Zn, N : TiO_2, zinc 2-ethylhexanoate [$C_{16}H_{30}O_4Zn$] in amounts 0.2, 0.5, 1.0 and 1.5 mol.% relative to [$Ti(OCH_2CH_2CH_2CH_3)_4$] was added to the precursor solution. However, throughout this article, the at.% of Zn doping, relative to Ti, as measured by EDS, is used to name a particular sample (*e.g.* 0.4% Zn, N : TiO_2 represents the sample where 0.2 mol.% of Zn precursor is added relative to the Ti precursor).

Aerosol-assisted chemical vapour deposition (AACVD) was used to deposit the films. A mist of precursor droplets was generated using an ultrasonic humidifier (2 MHz, Liquifog, Johnson Matthey) and was transferred to a heated reactor using a nitrogen carrier gas (BOC Ltd., 99.99%) with a flow rate of 1.4 L min^{-1}. The deposition was carried out at 500 °C for 40 min. After the deposition, the reactor was left to cool to room temperature under a flow of nitrogen gas before the film was removed.

Thin film characterisation

X-ray diffraction (XRD) patterns were measured using a modified Bruker-Axs D8 diffractometer with parallel beam optics and a PSD LynxEye silicon strip detector. The instrument uses a Cu source for X-ray generation (V = 40 kV, I = 30 mA) with Cu Kα1 (λ = 1.54056 Å) and Cu K α2 radiation (λ = 1.54439 Å) emitted with an intensity ratio of 2:1. The incident angle was set at 0.5° and the angular range of the patterns collected was $10° < 2\theta < 65°$ with a step size of 0.05° counted at 1 s/step. The General Structure Analysis System (GSAS) and Experiment Graphical user Interface (EXPGUI) suite were used to calculate the lattice parameters of all the thin films by fitting a Le Bail model to the XRD patterns.[31]

X-ray photoelectron spectroscopy (XPS) was performed using a Thermo Scientific K-alpha photoelectron spectrometer using monochromatic Al-K_α radiation. Survey scans were collected in the range 0–1100 eV (binding energy) at a pass energy of 160 eV. Higher resolution scans were recorded for the main core lines at a pass energy of 20 eV. Valence band spectra were also recorded. Peak positions were calibrated to adventitious carbon (284.5 eV) and analysed using CasaXPS software.

UV-visible transmission and reflection spectra were measured using a Perkin Elmer Fourier transform Lambda 950 spectrometer over a wavelength range of 250 – 2500 nm. The spectra were referenced against an air background. Films thickness was determined using a Filmetrics F20 thin film analyser.

Scanning Electron Microscopy (SEM) was used to determine surface morphology and film thickness using a JEOL JSM-6301F Field Emission SEM at an accelerating voltage of 5 keV.

Superoxide detection

A 100 μM solution of 2,3-bis(2-methoxy-4-nitro-5-sulfophenyl)-5-[(phenylamino)carbonyl]-2H-tetrazolium sodium salt (XTT) was used as the indicator for detecting superoxide ($^{\bullet}O_2^-$). Samples were cut (2 × 2 cm) and placed in a glass tube, following which; 2.5 ml of XTT was added.[32] Samples were maintained at room temperature for the testing period (~22 °C, 44 hrs). Float glass was used as a control. After various UVA illumination periods (365 nm, 3.15 $mW.cm^{-2}$), 1 mL of the solution was removed to measure the change in colour due to XTT's reduction to XTT-formazan (colourless to orange). The concentration of XTT-formazan was determined using a UV-visible absorption spectroscopy using the Beer-Lambert law:

$$c = A / (\varepsilon \times b) \qquad \text{(Eq. 1)}$$

where c is the concentration of XTT-formazan (M); A is the absorbance at 470 nm; ε is the wavelength-dependent extinction coefficient for XTT-formazan at 470 nm of $2.16 \times 10^4\ M^{-1}\ cm^{-1}$; and b is the path length of the cuvette (1 cm).[33]

Photocatalytic activity

Stearic acid (0.05 M, 95%, Sigma-Aldrich) in chloroform was used as a model organic pollutant for measuring photocatalytic activity.[34] Using a dip-coating method, photocatalyst films were coated with a thin layer of stearic acid; Pilkington NSG™

Activ™ glass was used as a benchmark and float glass as a control. The photocatalytic activity of the films was monitored by Fourier transform-infrared (FT-IR) spectroscopy using a PerkinElmer RX-I instrument. The IR spectrum of each acid overlayer was recorded over the range 3000–2700 cm^{-1}, and the areas of the peaks between 2950 and 2870 and 2870 and 2830 cm^{-1} were integrated. These peaks respectively represent the C–H antisymmetric and symmetric stretches of stearic acid and can be directly related to the concentration of stearic acid on the film's surface.[35] The samples were irradiated using a 365 nm ($I = 3.15\ mW\ cm^{-2}$) UV lamp. The IR spectrum of each acid-over layer was then recorded over the same range 3000–2700 cm^{-1}. The peaks between 3000 – 2700 cm^{-1} were integrated at each time interval, and converted to the number of stearic acid molecules per cm^{-2} using the conversion factor 9.7×10^{15} molecules = 1 $A.cm^{-1}$), allowing the reaction rate to be determined (molecules degraded.cm^{-2}.s^{-1}).[35] With knowledge of the photon flux (photons.cm^{-2}.s^{-1}), the formal quantum efficiency (FQE) was determined, which is defined as the molecules of stearic acid degraded per incident photon (molecules.$photon^{-1}$).

Bactericidal activity

One colony of *Escherichia coli* (ATCC 25922) was inoculated into 10 mL of brain heart infusion (BHI; Oxoid, Basingstoke, UK) and incubated with shaking at 200 rpm at 37 °C for 18 h. The culture was centrifuged at 3000 g for 15 min to recover the bacteria and washed in phosphate-buffered saline (PBS; 10 mL; Oxoid), then centrifuged at 3000 g for 15 min and resuspended in 10 mL of PBS. Finally, suspensions of the bacteria were diluted in 10 ml of PBS to give an inoculum containing approximately 1 x 10^6 colony-forming units (CFU/mL). The samples and control glass were cut into 2 × 2 cm pieces. Water (5 ml) was added to each petri dish to make a humid atmosphere and prevent the suspensions from drying out. A 25-µL aliquot of the bacterial cell suspension, *E. coli*, was spread evenly on the surface of each sample and incubated at room temperature for 8 h under UVA (365 nm) illumination and for 18 h under fluorescent light. The intensity of the fluorescent light was measured to range between 6000 and 9000 lux, at a distance of 30 cm from the lamp (28-W fluorescent lamp) using a lux meter (LX-101, Lutron Inc., Coopersburg, PA).

After incubation, the slides were transferred to 5 mL of PBS and vortexed for 40 s. Serial dilution of the resulting bacterial suspensions were prepared in PBS, and 100 μL from each dilution was spread onto MacConkey agar. All the plates were incubated for 24 h at 37 °C. After incubation, any bacterial colonies were counted, and viable counts of bacteria were determined.[36]

Transient absorption spectroscopy

Transient absorption spectroscopy (TAS), from the microsecond to second timescale, was measured in transmission mode. A Nd:YAG laser (OPOTEK Opolette 355 II, ~6 ns pulse width) was used as the excitation source, generating 355 nm UV light from the third harmonic (~1.0 $mJ.cm^{-2}$). The laser light was transmitted to the sample through a light guide and fired at a rate of 0.65 Hz. The probe light was a 100 W Bentham IL1 quartz halogen lamp. Long pass filters (Comar Instruments) were placed between the lamp and sample to minimize short wavelength irradiation of the sample. Transient changes in absorption in the sample was collected by a 2-inch diameter, 2-inch focal length lens, relayed to a monochromator (Oriel Cornerstone 130), and measured at select wavelengths between 450 - 1000 nm. Time-resolved changes were measured using a Si photodiode (Hamamatsu S3071) from the microsecond to second timescale. Data at times faster than 3.6 milliseconds was recorded by an oscilloscope (Tektronics DPO3012) after passing through an amplifier box (Costronics). Data slower than 3.6 milliseconds was simultaneously recorded on a National Instrument DAQ card (NI USB-6251). Each kinetic trace was obtained from the average of between 100 and 250 laser pulses. Acquisitions were triggered by a photodiode (Thorlabs DET10A) exposed to laser scatter. Data was acquired and processed using home-built software written in Labview. Samples were measured in air.

Results and Discussion

Nominally undoped, N : TiO_2 and a range of Zn, N : TiO_2 thin films were grown from the AACVD reaction of titanium butoxide, *tert*-butylamine (1.5 mmol), zinc 2-ethylhexanoate (0.2, 0.5, 1.0 and 1.5 mol.%, relative to the Ti source) and ethanol at 500 °C on glass substrates. All films were translucent, covered all of the substrate and had excellent adherence; passing the Scotch tape test.

For the films where 0.2, 0.5, 1.0 and 1.5 mol.% of the Zn precursor was added relative to the Ti precursor, energy dispersive X-ray spectroscopy (EDS) revealed the bulk Zn doping concentrations, relative to Ti, were 0.4, 1.0, 1.4 and 2.9 at.%, respectively. The presence of N could not be resolved due to the overlap of N K and Ti L lines in EDS spectra.

Nitrogen was however successfully detected from X-ray photoelectron spectroscopy (XPS) analysis, along with Ti and Zn, both on the surface and in the bulk of the films (**Figure 1 and Figure S1**). The N 1s region for the N : TiO_2 films showed a doublet of peaks centred at ~401.5 eV and ~399.1 eV (**Figure 1a**). The peak at ~401.5 eV matches to literature reports for nitric oxide (NO) species on TiO_2 that are reported at 401.9 eV.[22,37] Depth profiling of the films showed that the NO species were only present on the surface, with peaks disappearing after argon etch cycling **(Figure S1)**. These NO species are thought to arise from the oxidation of ammonium salt by-products during the CVD process.[14] The peak at ~399.1 eV, matches closely with literature values (~400 eV) for either chemisorbed N_2 species or interstitial N (N_i).[21] Here, the peak is assigned to N_i as it is present at both the surface (20-25% relative to Ti for all samples) and the bulk (6-11% relative to Ti). With respect to Zn, the Zn 2p regions showed a low signal to noise ratio, indicative of low concentrations at the surface, and therefore no fitting was applied to determine oxidation state (**Figure 1b**). The intensity of the Zn 2p signals did however increase with increased Zn doping, with a peak for the $2p_{3/2}$ found at ~1022 eV, which likely corresponds to Zn in the 2+ oxidation state.[38] Fitting of the Ti 2p region revealed Ti was in the 4+ oxidation state, evident from the Ti $2p_{3/2}$ peaks centred at ~458.0 eV (**Figure 1c**).[39] However, in the two samples, N : TiO_2 and 0.4 % Zn, N : TiO_2, an additional shoulder at ~456.0 eV, corresponding to the presence of Ti^{3+}, was also observed. The presence of reduced TiO_2 on the surface of these two samples is not entirely unexpected, as N doping is

known to induce oxygen vacancies. Computational studies have shown that the formation energy of oxygen vacancies significantly decreases with the introduction of N into the TiO_2 lattice, with this decrease attributed to a charge compensation effect.[14,40,41] Additionally, the formation of oxygen vacancies, and thus Ti^{3+} states, is further assisted by the reducing nature of the N precursor, *tert*-butylamine, used in this study, that is known to decompose at the temperatures used in our CVD reactions to produce the reducing gases NH_3 and CH_4.[42] Interestingly, at higher levels of Zn doping (1.0 at.% and above), the Ti^{3+} shoulder was not observed, which we attribute the higher levels of the oxygen rich Zn precursor, zinc 2-ethylhexanoate, used.

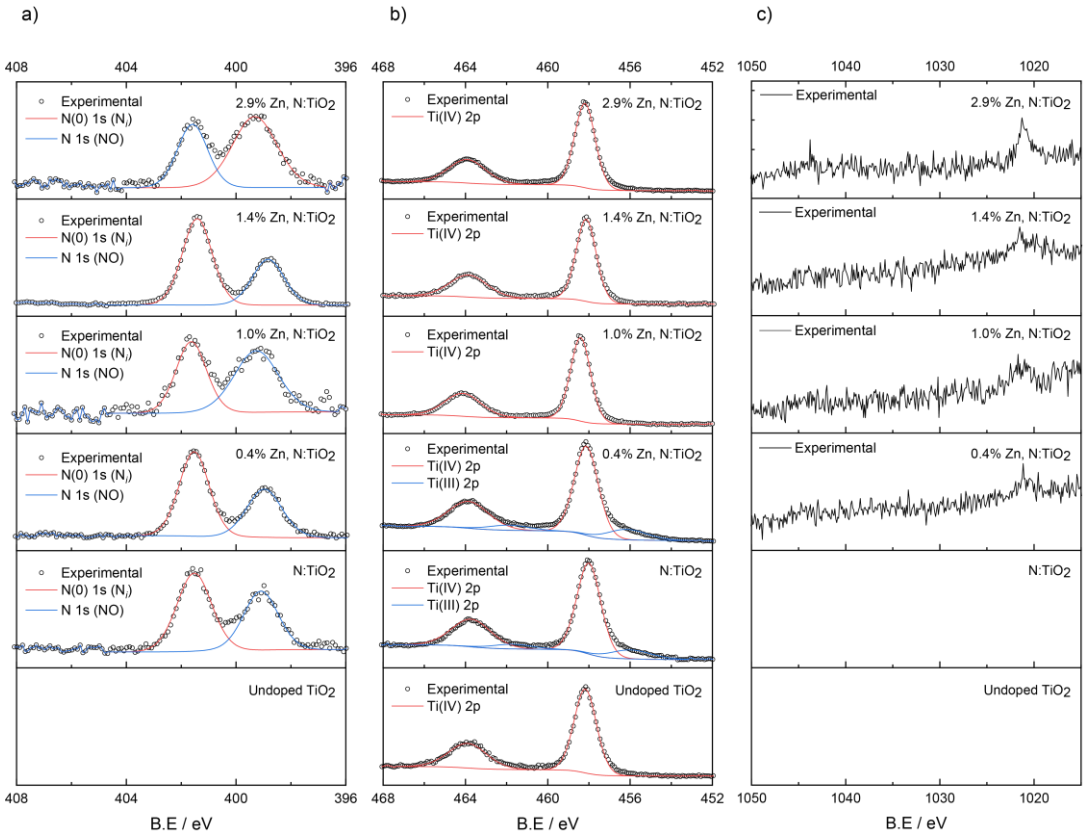

Figure 1: XPS spectra showing the a) N 1s, b) Ti 2p and c) Zn 2p regions of the nominally undoped TiO_2, N : TiO_2 and series of Zn, N : TiO_2 (Zn = 0.4 to 2.9 at.%) thin films grown *via* AACVD.

X-ray diffraction (XRD) of the nominally undoped TiO_2, N : TiO_2 and the Zn, N : TiO_2 films are presented in **Figure 2**. XRD patterns peaks for only anatase TiO_2 were observed, at 2θ values of 25.3, 38.6, 48.0, 55.1 and 62.8° that correspond with the (101), (112), (200), (211) and (204) Miller planes, respectively. A Le Bail model was fit to each XRD pattern to determine changes in the lattice parameters (**Table 1**). The nominally undoped TiO_2 had a unit cell volume of 136.21(5) $Å^3$, matching closely

with literature values of 136.25 $Å^3$.[43] Upon interstitial doping with N, in the N : TiO_2 sample, no significant expansion in the TiO_2 cell volume was observed. However, upon introduction of Zn, a slight expansion in the TiO_2 lattice was observed, increasing from 136.21(5) $Å^3$ in the undoped TiO_2 sample to 137.03(6) in the 1.0% Zn, N : TiO_2 sample. This is attributed to the introduction of Zn^{2+} (0.6 Å) ions that are larger than the Ti^{4+} (0.42 Å) ions that they likely replace. With respect to preferred orientation of the crystallographic planes, the undoped TiO_2 showed no preferential growth and the 0.4% Zn, N : TiO_2 showed higher than expected intensity (relative to the calculated pattern) for the (103), (004),(112), (105), (211) and (204) reflections, while the (101) and (200) showed reduced intensity. The remaining films all showed low intensity for the (103), (004), (112) and (204) peaks, while the (101) peak showed a slightly higher intensity than expected. The changes in preferred orientation are not unusual for metal oxide films grown on glass substrates.[44]

The changes in preferred orientation are not obviously reflected in the morphology of the films, as seen by scanning electron microscopy (SEM).

Raman spectroscopy is sensitive to the different phases of TiO_2 and thus used to probe phase purity of the films.[45] The spectra **(Figure 2b)** show peaks at 141.5 cm^{-1} (E_g), 397 cm^{-1} (B_{1g}), 514 cm^{-1} (A_{1g}) and 635 cm^{-1} (E_g) only, corresponded solely to the presence of anatase TiO_2**;** in agreement with XRD results.

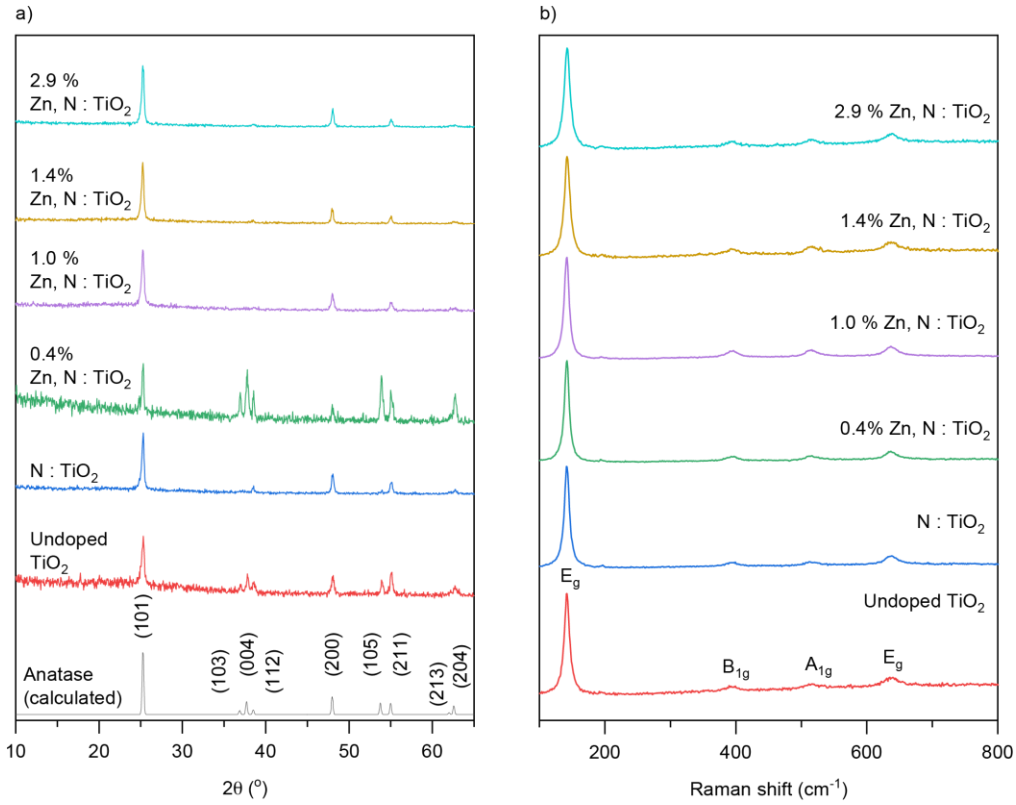

Figure 2: a) XRD patterns and b) Raman spectra of the nominally undoped TiO_2, N : TiO_2 and series of Zn, N : TiO_2 (Zn = 0.4 to 2.9 at.%) thin films grown *via* AACVD.

Table 1: Unit cell parameters, derived from Le Bail modelling of XRD patterns, of the nominally undoped TiO_2, N : TiO_2 and series of Zn, N : TiO_2 (Zn = 0.4 to 2.9 at.%) thin films grown *via* AACVD.

Sample	*a* /Å	*c* /Å	Unit cell volume /Å^3
Undoped TiO_2	3.785(1)	9.509(6)	136.21(5)
N : TiO_2	3.7866(7)	9.51(1)	136.35(8)
0.4% Zn, N : TiO_2	3.785(2)	9.523(6)	136.43(5)
1.0% Zn, N : TiO_2	3.789(1)	9.55(3)	137.03(6)
1.4% Zn, N : TiO_2	3.7867(7)	9.51(1)	136.35(7)
2.9% Zn, N : TiO_2	3.786(1)	9.55(3)	136.92(10)

SEM images show all films possess a needle like morphology (**Figure 3**). However as film thickness increases (~360, 420, 530, 550, 510 and 790 nm for the undoped TiO_2, N : TiO_2, 0.4% Zn, N : TiO_2, 1.0% Zn, N : TiO_2, 1.4% Zn, N : TiO_2, and 2.9% Zn,

N : TiO_2 films, respectively), the randomly aligned needles across the horizontal appear to coalesce to give a flatter and more featureless surface. The surface morphology and surface area can have a substantial impact on the photocatalytic activity.[46] Generally, the more featured the morphology, the larger the surface area and photocatalytic/bactericidal activity due to more of the active area exposed to the surrounding environment.

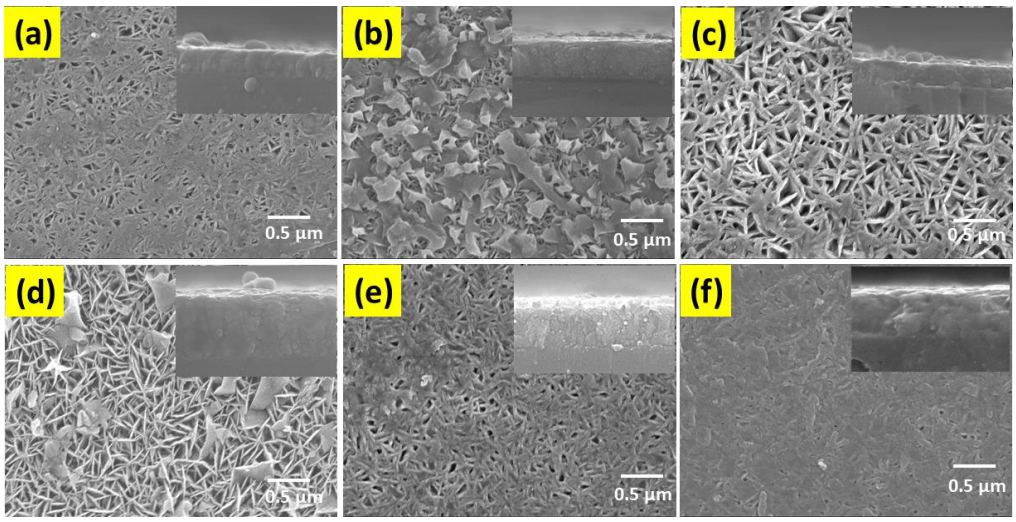

Figure 3: SEM images of a) undoped TiO_2, b) N : TiO_2, c) 0.4% Zn, N : TiO_2, d) 1.0% Zn, N : TiO_2, e) 1.4% Zn, N : TiO_2, and f) 2.9% Zn, N : TiO_2 thin films.

The transmittance and reflectance spectra of the various TiO_2 based films are shown in **Figure 4a**. All films showed reasonable optical transparency (~65%) and reflectance (<20%) across the visible region (400 - 800 nm). The indirect-allowed optical bandgaps were determined from Tauc plots, as shown in **Figure 4b**. The nominally undoped TiO_2 film showed the expected bandgap of 3.3 eV, which remained the same upon N doping, as expected with interstitial doping.[14] Zn doping of N : TiO_2 caused a marginal decrease in the optical bandgap.

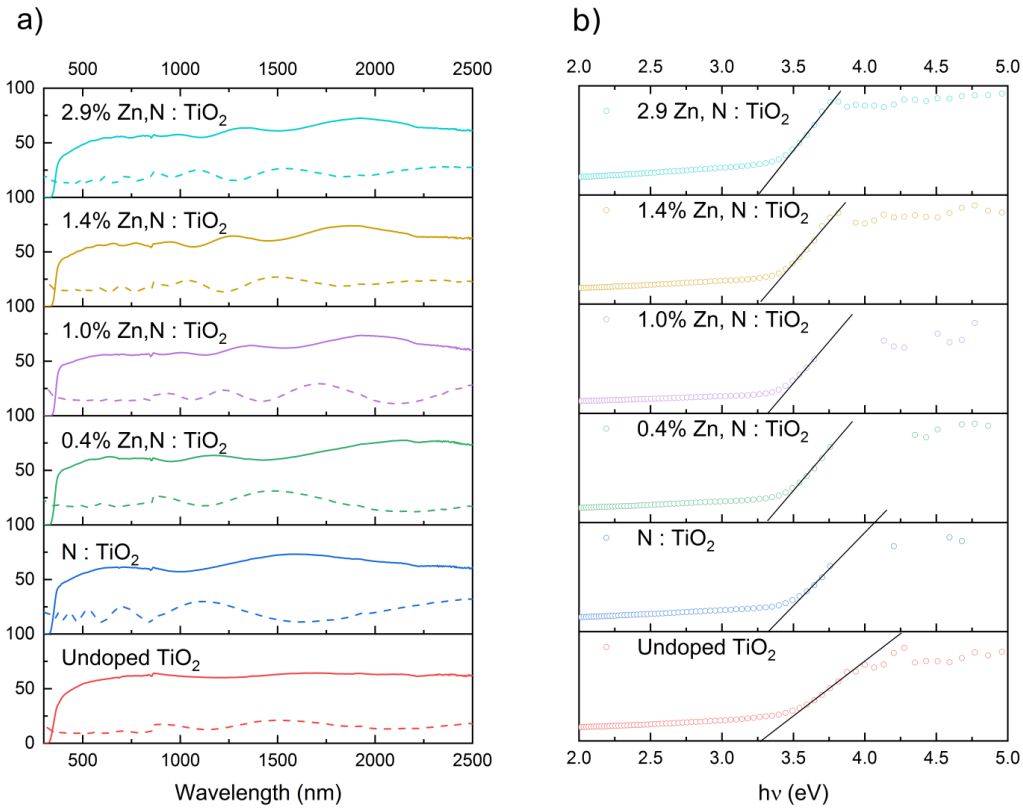

Figure 4: a) UV/vis spectra and b) corresponding Tauc plots showing an indirect optical bandgap of 3.27, 3.30, 3.30, 3.31, 3.26 and 3.26 eV for the undoped TiO_2, N : TiO_2, 0.4% Zn, N : TiO_2, 1.0% Zn, N : TiO_2, 1.4% Zn, N : TiO_2, and 2.9% Zn, N : TiO_2 thin films grown in this study.

Reactive oxygen species (ROS), like superoxide ($^{\bullet}O_2^-$), singlet oxygen ($^1O_2$) and hydroxyl radicals ($^{\bullet}OH$) play an important role in both photocatalytic cleaning of organic contaminants as well as bactericidal activity.[47–49] In this study, the generation of the superoxide anion radical ($^{\bullet}O_2^-$), under the action of UVA light, was investigated using XTT sodium salt. Absorbance at 470 nm, after 44 hrs of UVA light, shows that the 100 µM XTT salt was reduced to XTT formazan by the superoxide radical ($^{\bullet}O_2^-$), as shown in **Figure S2 in the ESI**. This reduction did not occur in the blank. **Figure S3 in the ESI** shows that all films generate $^{\bullet}O_2^-$ under UVA light. **Figure 5** shows the amount of $^{\bullet}O_2^-$ formation with time for all samples. The 0.4 and 1.4% Zn, N : TiO_2 showed the highest amount of $^{\bullet}O_2^-$ formation, while the 2.9% Zn, N : TiO_2 film showed the lowest.

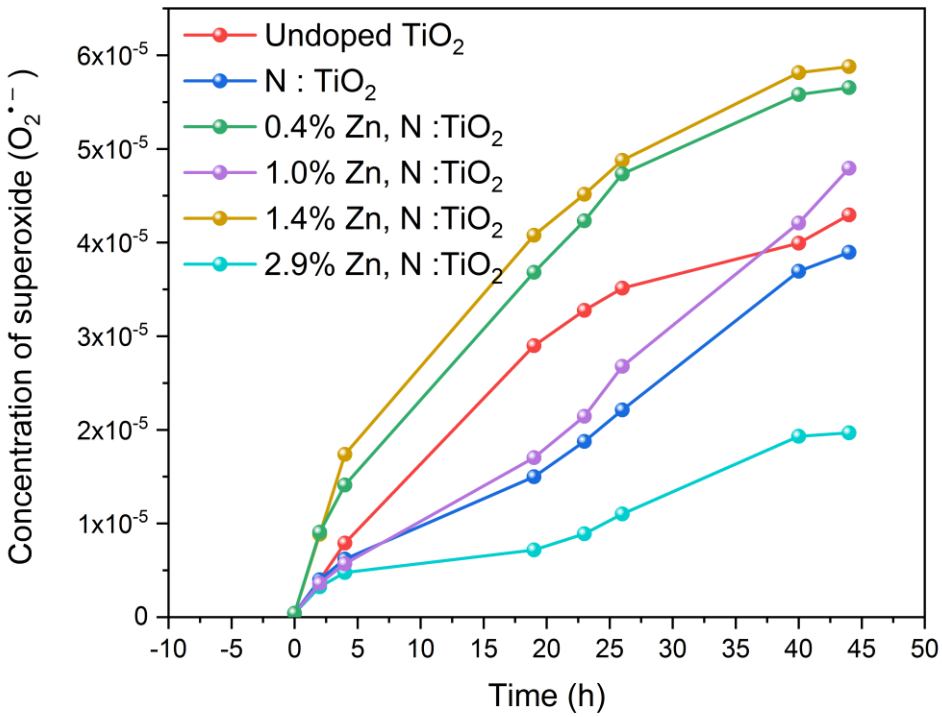

Figure 5: The concentration of superoxide ($^{\bullet}O_2^-$) formed over time (hours) under UVA illumination for undoped TiO_2, N : TiO_2, and series of Zn, N : TiO_2 (Zn = 0.4 to 2.9 at.%) thin films.

The photocatalytic activities of undoped TiO_2, N : TiO_2 and the series of Zn, N : TiO_2 (Zn = 0.4 to 2.9 at. %) thin films were investigated using the model organic pollutant, stearic acid, under UVA irradiation.[50,51] Activ™ glass, a commercially available self-cleaning glass, was used as a benchmark for comparison. No change in stearic acid concentration was observed on the glass blank, which showed that loss of stearic acid in our thin films was due to semiconductor sensitised photocatalysis.

Photocatalytic rates were determined from the initial rate of decay (linear regression of the initial 30 - 40% of the curve of integrated area versus illumination time) (**Figure 6**). The undoped TiO_2 film exhibited a formal quantum efficiency (FQE) of 1.5×10^{-5} molecules.photon^{-1}. A slightly higher FQE of 2.1×10^{-5} molecules.photon^{-1} was found in the N : TiO_2 film. Upon Zn doping, the FQE initially increased, with 0.4% Zn, N : TiO_2 and 1.0% Zn, N : TiO_2 showing substantially higher FQE values of 3.3×10^{-5} and 2.5×10^{-5} molecules.photon^{-1}, respectively. However, at higher Zn doping levels, the FQE decreased, with 1.4% Zn, N : TiO_2 and 2.9% Zn, N : TiO_2 showing 7.0×10^{-6} and 3.0×10^{-6} molecules.photon^{-1}, respectively. This could be due

to a number of reasons, including the flatter surface morphology observed for the higher doped samples (1.4, 2.9 at.% Zn). Importantly, the 0.4% Zn, N : TiO_2 displayed more than twice the FQE of undoped TiO_2, and 65% higher activity than the commercial standard, Activ^{TM} (2.0×10^{-4} molecules.photon^{-1}). Interestingly, these photocatalytic activities correlated well with the amount of $^{\bullet}O_2^-$ generated (**Figure 5**). For instance, 0.4% Zn, N : TiO_2 exhibited the second highest $^{\bullet}O_2^-$ generation rate and highest photocatalytic, whereas 2.9% Zn, N : TiO_2 exhibited the lowest $O_2^{\bullet -}$ generation and lowest photocatalytic activity. This result supports the general photocatalysis mechanism in which organics are oxidised by TiO_2,[5] where photogenerated electrons and holes react respectively with O_2 and H_2O to form $^{\bullet}O_2^-$ and $^{\bullet}OH$ radicals that degrade organic species.[52,53]

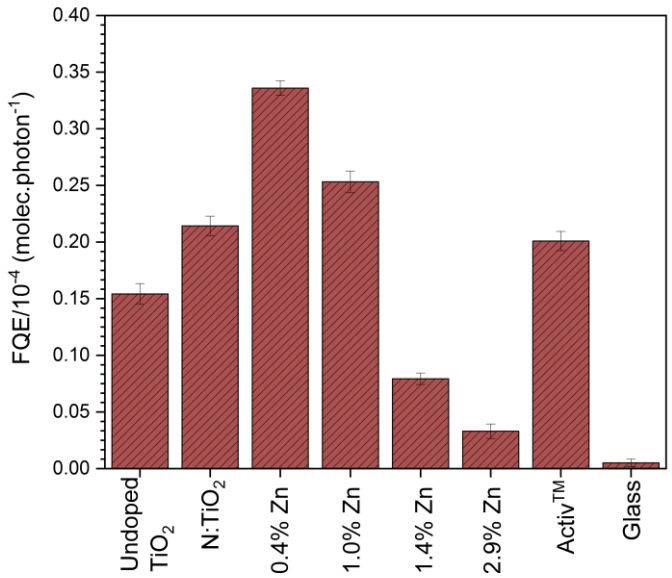

Figure 6: Formal quantum efficiencies (FQE) of the photocatalytic degradation of stearic acid under UVA light for undoped TiO_2, N : TiO_2 and series of Zn, N : TiO_2 (Zn = 0.4 to 2.9 at.%) thin films grown *via* AACVD. For comparison, a commercial self-cleaning glass, Activ^{TM}, and glass blank were also examined.

Bactericidal tests of undoped TiO_2, N : TiO_2 and Zn, N : TiO_2 (Zn = 0.4 to 2.9 at.%) thin films were performed against the Gram-negative bacterium, *E. coli*. Bactericidal activity was determined by incubating the samples with bacteria at 37 °C for 8 under UVA or 18 hours under fluorescent light. Fluorescent light was also investigated for the antibacterial study, as this light source also irradiates in the UVA region and is comparable to that found in a clinical environment, such as operating theatres, in UK hospitals

The Zn, N : TiO_2 films demonstrated higher bactericidal activity compared with undoped TiO_2. **Figure 7a**, shows the viable counts of bacteria after incubation of the samples under UVA irradiation (I = 3.15 mW.cm^{-2}) and under dark conditions for 8 hrs. All films showed a significant reduction in the number of viable bacteria under UVA irradiation; in contrast, no significant reduction was observed in the dark. The 1.0% Zn, N : TiO_2 film showed the highest bactericidal activity under UVA for 8 hrs, followed by 1.4% Zn, N : TiO_2 and 0.4% Zn, N : TiO_2.

Figure 7b shows that Zn, N : TiO_2 films significantly reduced the viable counts of bacteria under fluorescent light (18 hrs). This was possible, despite the bandgaps (3.3 eV) of our films being in the UV region, due the fluorescent light source emitting some light in the UVA region, as shown in previous work.[54] The 1.0% Zn, N : TiO_2 film showed the highest bactericidal activity (3 log kill), followed by 0.4% Zn, N : TiO_2 (2 log kill). Undoped TiO_2 and N : TiO_2 showed less than 0.5 log kill under fluorescent light.

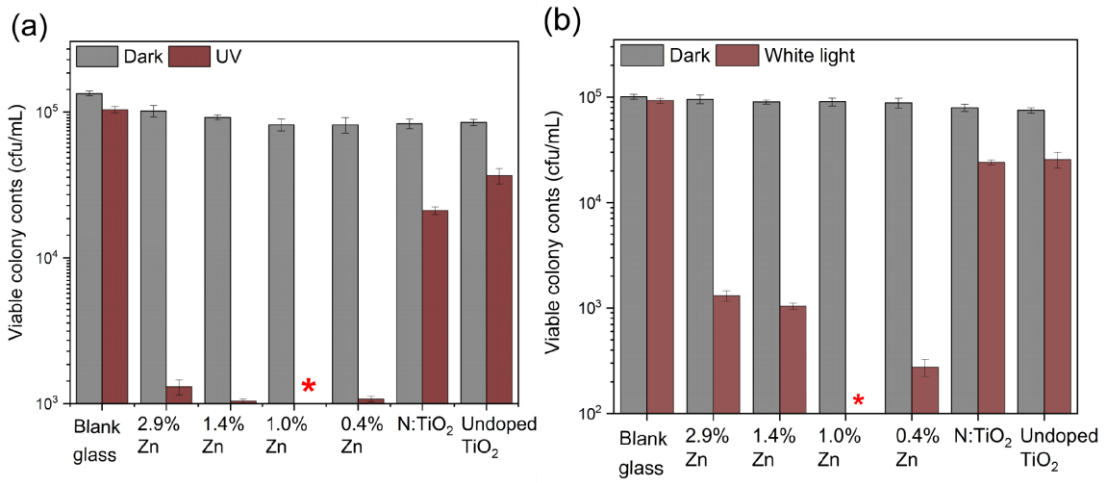

Figure 7: Viable counts of bacteria, after incubation under illumination in (a) UVA (8 hrs) and (b) fluorescent light (18 hrs) for undoped TiO_2, N : TiO_2 and series of Zn, N : TiO_2 (Zn = 0.4 to 2.9 at.%) thin films grown *via* AACVD. A glass blank was also examined for comparison.

Transient absorption spectroscopy (TAS) can measure charge carrier behaviour in photocatalytic coatings.[46,55–57] Following a supra-bandgap laser pulse, photogenerated electrons and holes are formed, and can be measured using time-resolved UV-visible absorption spectroscopy.

Transient decay dynamics (**Figures S3 & S4**) and absorption spectra (**Figures S5 & S6**) were measured for undoped TiO_2, N : TiO_2 and the series of Zn, N : TiO_2 films. Samples were excited using a UVA laser pulse (355 nm, ~1 $mJ.cm^{-2}$.per pulse), and transient changes in absorption were measured from 10 μs after the laser pulse to 1 s, over the range of wavelengths, 450 - 1000 nm. Transient decays represent the intrinsic electron-hole recombination dynamics present in these materials. The transient absorption spectra and decay dynamics of the undoped anatase TiO_2 films are similar to previous studies, showing broad absorption across the visible region and power law decay dynamics.[46] N doping decreased the recombination rate, showing a $t_{50\%}$ (time taken for half the signal to decay) of ~ 300 μs (**Figure S4**), similar to previous studies of this material.[22] Undoped TiO_2 and the series of Zn, N : TiO_2 showed similar recombination rates ($t_{50\%}$ ~ 100 μs). However, the transient absorption signals were significantly higher in Zn, N : TiO_2 samples, compared with N : TiO_2 or undoped TiO_2. For instance, at the probe wavelength of 500 nm, the 1.0% Zn, N : TiO_2 sample showed an absorption signal of ~1.35 mΔO.D, 10 μs after the laser pulse, whereas undoped TiO_2 showed an absorption signal of ~0.21 mΔO.D (**Figure S6**). Given transient absorption signals in the blue region of the electromagnetic spectrum typically represent hole carriers in TiO_2[46], this likely represents a more than six-fold increase in hole carrier population in the 1.0% Zn, N : TiO_2, compared with undoped TiO_2. This was attributed to inhibited, pre-μs recombination, rather than an increase in light absorption and carrier generation (as light absorption at 355 nm was similar in all samples, **Figure 4a**). In addition, the decay dynamics in Zn, N : TiO_2 was bi-phasic, and did not follow a simple power law decay, like undoped TiO_2 (**Figures S3 & S4**). Similar behaviour was previous observed in brookite TiO_2,[55] and was attributed to a wider distribution of trap state energies within the bandgap, resulting in a greater proportion of longer-lived charge carriers.

Given the Zn, N : TiO_2 films showed higher initial transient absorption than undoped TiO_2, due to inhibited pre-μs recombination, and recombined at a similar rate from the μs to s, we could rationalise the increase in photocatalytic activities observed herein. For instance, the general mechanism of photocatalysis proceeds with the reduction of O_2 to $^{\bullet}O_2^-$ by photogenerated electrons and oxidation of H_2O to $^{\bullet}OH$ by photogenerated holes. The kinetics of these processes are slow, and typically take place on the ms to s timescale.[6,58] On the ms timescale, Zn, N : TiO_2 films show

significantly higher transient absorption signals across the visible than undoped TiO_2 or N : TiO_2 (**Figure S5**). For instance, one of the most active photocatalysts, 1.0% Zn, N : TiO_2, shows, on average, a five-fold higher transient absorption signal, 1 ms after the laser pulse, than undoped TiO_2. Given the Zn, N : TiO_2 films show significantly higher transient absorption signals on timescales in which photocatalysis takes place, and that these transient absorption signals are directly proportional to the number of photogenerated charge carriers,[58,59] we use this to rationalise the higher levels of superoxide formation, photocatalytic and bactericidal activity observed herein.

Conclusion

Undoped TiO_2, N : TiO_2 and a series of Zn, N : TiO_2 (Zn = 0.4 to 2.9 at.%) thin films were grown by AACVD on glass substrates. Enhanced photocatalytic activity under UVA light was achieved for the destruction of stearic acid when co-doped with Zn and N, as compared with N doping or no doping. In addition, good bactericidal activity was observed for killing *E. coli* under UVA and fluorescent light. The generation of superoxide ($^{\bullet}O_2^-$) radicals from the surfaces of the samples was investigated using the reduction of XTT sodium salt under UVA irradiation. An increased concentration of superoxide formation from the Zn, N : TiO_2 thin films was observed and correlated with increases in bactericidal activity. TAS was used to study the recombination kinetics and lifetime, and showed that charge carrier populations increased when films were co-coped with Zn and N.

These Zn, N : TiO_2 coatings, produced by the scalable method of AACVD, have the potential to be used in a clinical environment as self-sterilising surfaces, functioning with indoor fluorescent lighting, and can also be implemented outdoors as self-cleaning and self-sterilising coatings, functioning with UV light contained in sunlight.

Acknowledgements

A. K. thanks Imperial College for a Junior Research Fellowship, the EPSRC for a Capital Award Emphasising Support for Early Career Researchers and the Royal

Society for an Equipment Grant (RSG\R1\180434). IPP and AMA are grateful to King Abdulaziz City for Science and Technology (KACST), Saudi Arabia for the provision of a PhD studentship to Abdullah Alotaibi and for financial support from the Saudi Cultural Bureau in London.

Supporting information

EDS results (Table S1); structural change of XTT to XTT formazan schematic (Figure S1); UV-Vis spectra of XTT on Zn, N doped TiO_2 films under UVA irradiation (Figure S2), TAS decay results (Figure S3-S6)

References

(1) Asahi, R.; Morikawa, T.; Irie, H.; Ohwaki, T. Nitrogen-Doped Titanium Dioxide as Visible-Light-Sensitive Photocatalyst: Designs, Developments, and Prospects. *Chem. Rev.* **2014**, *114* (19), 9824–9852.

(2) Hashimoto, K.; Irie, H.; Fujishima, A. TiO2 Photocatalysis: A Historical Overview and Future Prospects. *Jpn. J. Appl. Phys.* **2005**, *44* (12R), 8269.

(3) Linsebigler, A. L.; Lu, G.; Yates Jr, J. T. Photocatalysis on TiO2 Surfaces: Principles, Mechanisms, and Selected Results. *Chem. Rev.* **1995**, *95* (3), 735–758.

(4) McCullagh, C.; Robertson, J. M. C.; Bahnemann, D. W.; Robertson, P. K. J. The Application of TiO 2 Photocatalysis for Disinfection of Water Contaminated with Pathogenic Micro-Organisms: A Review. *Res. Chem. Intermed.* **2007**, *33* (3–5), 359–375.

(5) Mills, A.; Le Hunte, S. An Overview of Semiconductor Photocatalysis. *J. Photochem. Photobiol. A Chem.* **1997**, *108* (1), 1–35.

(6) Fujishima, A.; Zhang, X.; Tryk, D. TiO2 Photocatalysis and Related Surface Phenomena. *Surf. Sci. Rep.* **2008**, *63* (12), 515–582.

(7) Liu, Y.; Wang, X.; Yang, F.; Yang, X. Excellent Antimicrobial Properties of Mesoporous Anatase TiO2 and Ag/TiO2 Composite Films. *Microporous Mesoporous Mater.* **2008**, *114* (1–3), 431–439.

(8) Li, Y.; Zhang, W.; Niu, J.; Chen, Y. Mechanism of Photogenerated Reactive Oxygen Species and Correlation with the Antibacterial Properties of Engineered Metal-Oxide Nanoparticles. *ACS Nano* **2012**, *6* (6), 5164–5173.

(9) Wang, D.; Zhao, L.; Ma, H.; Zhang, H.; Guo, L.-H. Quantitative Analysis of Reactive Oxygen Species Photogenerated on Metal Oxide Nanoparticles and Their Bacteria Toxicity: The Role of Superoxide Radicals. *Environ. Sci. Technol.* **2017**, *51* (17), 10137–10145.

(10) Cadet, J.; Delatour, T.; Douki, T.; Gasparutto, D.; Pouget, J.-P.; Ravanat, J.-L.; Sauvaigo, S. Hydroxyl Radicals and DNA Base Damage. *Mutat. Res. Mol. Mech. Mutagen.* **1999**, *424* (1–2), 9–21.

(11) Sotelo-Vazquez, C.; Noor, N.; Kafizas, A.; Quesada-Cabrera, R.; Scanlon, D. O.; Taylor, A.; Durrant, J. R.; Parkin, I. P. Multifunctional P-Doped TiO2 Films: A New Approach to Self-Cleaning, Transparent Conducting Oxide Materials. *Chem. Mater.* **2015**, *27* (9), 3234–3242.

(12) Zhao, J.; Zhang, B.; Li, J.; Liu, Y.; Wang, W. Photo-Enhanced Oxidizability of Tetrazolium Salts and Its Impact on Superoxide Assaying. *Chem. Commun.* **2016**, *52* (77), 11595–11598.

(13) Zhao, Y.; Jafvert, C. T. Environmental Photochemistry of Single Layered Graphene Oxide in Water. *Environ. Sci. Nano* **2015**, *2* (2), 136–142.

(14) Di Valentin, C.; Finazzi, E.; Pacchioni, G.; Selloni, A.; Livraghi, S.; Paganini, M. C.; Giamello, E. N-Doped TiO2: Theory and Experiment. *Chem. Phys.* **2007**, *339* (1–3), 44–56.

(15) Zaleska, A. Doped-TiO2: A Review. *Recent patents Eng.* **2008**, *2* (3), 157–164.

(16) Jagadale, T. C.; Takale, S. P.; Sonawane, R. S.; Joshi, H. M.; Patil, S. I.; Kale, B. B.; Ogale, S. B. N-Doped TiO2 Nanoparticle Based Visible Light Photocatalyst by Modified Peroxide Sol− Gel Method. *J. Phys. Chem. C* **2008**, *112* (37), 14595–14602.

(17) Nakamura, R.; Tanaka, T.; Nakato, Y. Mechanism for Visible Light Responses in Anodic Photocurrents at N-Doped TiO2 Film Electrodes. *J. Phys. Chem. B*

2004, *108* (30), 10617–10620.

(18) Sathasivam, S.; Bhachu, D. S.; Lu, Y.; Chadwick, N.; Althabaiti, S. A.; Alyoubi, A. O.; Basahel, S. N.; Carmalt, C. J.; Parkin, I. P. Tungsten Doped TiO2 with Enhanced Photocatalytic and Optoelectrical Properties via Aerosol Assisted Chemical Vapor Deposition. *Sci. Rep.* **2015**, *5*.

(19) Tang, J.; Cowan, A. J.; Durrant, J. R.; Klug, D. R. Mechanism of O2 Production from Water Splitting: Nature of Charge Carriers in Nitrogen Doped Nanocrystalline TiO2 Films and Factors Limiting O2 Production. *J. Phys. Chem. C* **2011**, *115* (7), 3143–3150.

(20) Kafizas, A.; Dunnill, C. W.; Parkin, I. P. Combinatorial Atmospheric Pressure Chemical Vapour Deposition (CAPCVD) of Niobium Doped Anatase; Effect of Niobium on the Conductivity and Photocatalytic Activity. *J. Mater. Chem.* **2010**, *20* (38), 8336–8349.

(21) Kafizas, A.; Crick, C.; Parkin, I. P. The Combinatorial Atmospheric Pressure Chemical Vapour Deposition (CAPCVD) of a Gradating Substitutional/Interstitial N-Doped Anatase TiO2 Thin-Film; UVA and Visible Light Photocatalytic Activities. *J. Photochem. Photobiol. A Chem.* **2010**, *216* (2–3), 156–166.

(22) Chadwick, N. P.; Kafizas, A.; Quesada-Cabrera, R.; Sotelo-Vazquez, C.; Bawaked, S. M.; Mokhtar, M.; Al Thabaiti, S. A.; Obaid, A. Y.; Basahel, S. N.; Durrant, J. R. Ultraviolet Radiation Induced Dopant Loss in a TiO2 Photocatalyst. *ACS Catal.* **2017**, *7* (2), 1485–1490.

(23) Zhao, Y.; Li, C.; Liu, X.; Gu, F.; Du, H. L.; Shi, L. Zn-Doped TiO2 Nanoparticles with High Photocatalytic Activity Synthesized by Hydrogen–Oxygen Diffusion Flame. *Appl. Catal. B Environ.* **2008**, *79* (3), 208–215.

(24) Zhang, W.; Zhu, S.; Li, Y.; Wang, F. Photocatalytic Zn-Doped TiO2 Films Prepared by DC Reactive Magnetron Sputtering. *Vacuum* **2007**, *82* (3), 328–335.

(25) Hassan, I. A.; Sathasivam, S.; Nair, S. P.; Carmalt, C. J. Antimicrobial Properties of Copper-Doped ZnO Coatings under Darkness and White Light

Illumination. *ACS omega* **2017**, *2* (8), 4556–4562.

(26) Jaiswal, R.; Bharambe, J.; Patel, N.; Dashora, A.; Kothari, D. C.; Miotello, A. Copper and Nitrogen Co-Doped TiO2 Photocatalyst with Enhanced Optical Absorption and Catalytic Activity. *Appl. Catal. B Environ.* **2015**, *168*, 333–341.

(27) Xu, Z.; Yang, W.; Li, Q.; Gao, S.; Shang, J. K. Passivated n–p Co-Doping of Niobium and Nitrogen into Self-Organized TiO2 Nanotube Arrays for Enhanced Visible Light Photocatalytic Performance. *Appl. Catal. B Environ.* **2014**, *144*, 343–352.

(28) Powell, M. J.; Carmalt, C. J. Aerosols: A Sustainable Route to Functional Materials. *Chem. - A Eur. J.* **2017**, *23* (62), 15543–15552.

(29) Sathasivam, S.; Williamson, B. A. D.; Althabaiti, S. A.; Obaid, A. Y.; Basahel, S. N.; Mokhtar, M.; Scanlon, D. O.; Carmalt, C. J.; Parkin, I. P. Chemical Vapor Deposition Synthesis and Optical Properties of Nb2O5 Thin Films with Hybrid Functional Theoretical Insight into the Band Structure and Band Gaps. *ACS Appl. Mater. Interfaces* **2017**, *9* (21), 18031–18038.

(30) Sathasivam, S.; Williamson, B. A. D.; Kafizas, A.; Althabaiti, S. A.; Obaid, A. Y.; Basahel, S. N.; Scanlon, D. O.; Carmalt, C. J.; Parkin, I. P. Computational and Experimental Study of Ta2O5 Thin Films. *J. Phys. Chem. C* **2017**, *121* (1), 202–210.

(31) Toby, B. H. EXPGUI, a Graphical User Interface for GSAS. *J. Appl. Crystallogr.* **2001**, *34* (2), 210–213.

(32) Li, X. Z.; Li, F. B.; Yang, C. L.; Ge, W. K. Photocatalytic Activity of WOx-TiO2 under Visible Light Irradiation. *J. Photochem. Photobiol. A Chem.* **2001**, *141* (2–3), 209–217.

(33) Able, A. J.; Guest, D. I.; Sutherland, M. W. Use of a New Tetrazolium-Based Assay to Study the Production of Superoxide Radicals by Tobacco Cell Cultures Challenged with Avirulent Zoospores OfPhytophthora Parasitica Varnicotianae. *Plant Physiol.* **1998**, *117* (2), 491–499.

(34) Mills, A.; Wang, J. Simultaneous Monitoring of the Destruction of Stearic Acid

and Generation of Carbon Dioxide by Self-Cleaning Semiconductor Photocatalytic Films. *J. Photochem. Photobiol. A Chem.* **2006**, *182* (2), 181–186.

(35) Mills, A.; McFarlane, M. Current and Possible Future Methods of Assessing the Activities of Photocatalyst Films. *Catal. Today* **2007**, *129* (1), 22–28.

(36) Alotaibi, A. M.; Sathasivam, S.; Nair, S. P.; Parkin, I. P. Antibacterial Properties of Cu–ZrO 2 Thin Films Prepared via Aerosol Assisted Chemical Vapour Deposition. *J. Mater. Chem. B* **2016**, *4* (4), 666–671.

(37) Palgrave, R. G.; Payne, D. J.; Egdell, R. G. Nitrogen Diffusion in Doped TiO 2 (110) Single Crystals: A Combined XPS and SIMS Study. *J. Mater. Chem.* **2009**, *19* (44), 8418–8425.

(38) Wehner, P. S.; Mercer, P. N.; Apai, G. Interaction of H2 and CO with Rh4 (CO) 12 Supported on ZnO. *J. Catal.* **1983**, *84* (1), 244–247.

(39) Biesinger, M. C.; Lau, L. W. M.; Gerson, A. R.; Smart, R. S. C. Resolving Surface Chemical States in XPS Analysis of First Row Transition Metals, Oxides and Hydroxides: Sc, Ti, V, Cu and Zn. *Appl. Surf. Sci.* **2010**, *257* (3), 887–898.

(40) Di Valentin, C.; Pacchioni, G.; Selloni, A. Reduced and N-Type Doped TiO2: Nature of Ti3+ Species. *J. Phys. Chem. C* **2009**, *113* (48), 20543–20552.

(41) Di Valentin, C.; Pacchioni, G.; Selloni, A.; Livraghi, S.; Giamello, E. Characterization of Paramagnetic Species in N-Doped TiO2 Powders by EPR Spectroscopy and DFT Calculations. *J. Phys. Chem. B* **2005**, *109* (23), 11414–11419.

(42) Pritchard, H. O.; Sowden, R. G.; Trotman-Dickenson, A. F. The Thermal Decomposition of Tert.-Butylamine. *J. Chem. Soc.* **1954**, 546–549.

(43) Horn, M.; Schwebdtfeger, C. F.; Meagher, E. P. Refinement of the Structure of Anatase at Several Temperatures. *Zeitschrift für Krist. Mater.* **1972**, *136* (1–6), 273–281.

(44) Ghosh, R.; Basak, D.; Fujihara, S. Effect of Substrate-Induced Strain on the

Structural, Electrical, and Optical Properties of Polycrystalline ZnO Thin Films. *J. Appl. Phys.* **2004**, *96* (5), 2689–2692.

(45) Zhang, J.; Li, M.; Feng, Z.; Chen, J.; Li, C. UV Raman Spectroscopic Study on TiO2. I. Phase Transformation at the Surface and in the Bulk. *J. Phys. Chem. B* **2006**, *110* (2), 927–935.

(46) Wang, X.; Kafizas, A.; Li, X.; Moniz, S. J. A.; Reardon, P. J. T.; Tang, J.; Parkin, I. P.; Durrant, J. R. Transient Absorption Spectroscopy of Anatase and Rutile: The Impact of Morphology and Phase on Photocatalytic Activity. *J. Phys. Chem. C* **2015**, *119* (19), 10439–10447.

(47) Fang, F. C. Antimicrobial Actions of Reactive Oxygen Species. *MBio* **2011**, *2* (5).

(48) Nosaka, Y.; Nosaka, A. Y. Generation and Detection of Reactive Oxygen Species in Photocatalysis. *Chem. Rev.* **2017**, *117* (17), 11302–11336.

(49) Yu, T.; Liu, Z.; Ma, J.; Tan, X. The Photocatalytic Oxidation of As (III) Enhanced by Surface Alkalinized GC 3 N 4. *Trans. Tianjin Univ.* **2020**, *26* (1), 40–48.

(50) Cabrera, R. Q.; Latimer, E. R.; Kafizas, A.; Blackman, C. S.; Carmalt, C. J.; Parkin, I. P. Photocatalytic Activity of Needle-like TiO2/WO3− x Thin Films Prepared by Chemical Vapour Deposition. *J. Photochem. Photobiol. A Chem.* **2012**, *239*, 60–64.

(51) Bhachu, D. S.; Sathasivam, S.; Carmalt, C. J.; Parkin, I. P. PbO-Modified TiO2 Thin Films: A Route to Visible Light Photocatalysts. *Langmuir* **2014**, *30* (2), 624–630.

(52) Jenny, S.; Masaya, M.; Masato, T.; Jinlong, Z.; Yu, H.; Masakazu, A.; Bahnemann, D. W. *Understanding TiO2 Photocatalysis: Mechanisms and Materials*; 2014; Vol. 114.

(53) Augugliaro, V.; Litter, M.; Palmisano, L.; Soria, J. The Combination of Heterogeneous Photocatalysis with Chemical and Physical Operations: A Tool for Improving the Photoprocess Performance. *J. Photochem. Photobiol. C*

Photochem. Rev. **2006**, *7* (4), 127–144.

(54) Kafizas, A.; Kellici, S.; Darr, J. A.; Parkin, I. P. Titanium Dioxide and Composite Metal/Metal Oxide Titania Thin Films on Glass: A Comparative Study of Photocatalytic Activity. *J. Photochem. Photobiol. A Chem.* **2009**, *204* (2), 183–190.

(55) Moss, B.; Lim, K. K.; Beltram, A.; Moniz, S.; Tang, J.; Fornasiero, P.; Barnes, P.; Durrant, J.; Kafizas, A. Comparing Photoelectrochemical Water Oxidation, Recombination Kinetics and Charge Trapping in the Three Polymorphs of TiO2. *Sci. Rep.* **2017**, *7* (1), 2938.

(56) Sotelo-Vazquez, C.; Quesada-Cabrera, R.; Ling, M.; Scanlon, D. O.; Kafizas, A.; Thakur, P. K.; Lee, T.; Taylor, A.; Watson, G. W.; Palgrave, R. G. Evidence and Effect of Photogenerated Charge Transfer for Enhanced Photocatalysis in WO3/TiO2 Heterojunction Films: A Computational and Experimental Study. *Adv. Funct. Mater.* **2017**, *27* (18), 1605413.

(57) Kafizas, A.; Wang, X.; Pendlebury, S. R.; Barnes, P. R. F.; Ling, M.; Sotelo-Vazquez, C.; Quesada-Cabrera, R.; Li, C.; Parkin, I. P.; Durrant, J. R. Where Do Photo-Generated Holes Go in Anatase:Rutile TiO2? A Transient Absorption Spectroscopy Study of Charge Transfer and Lifetime. *J. Phys. Chem. A* **2016**, *120* (5), 715–723.

(58) Kafizas, A.; Ma, Y.; Pastor, E.; Pendlebury, S. R.; Mesa, C.; Francàs, L.; Le Formal, F.; Noor, N.; Ling, M.; Sotelo-Vazquez, C. Water Oxidation Kinetics of Accumulated Holes on the Surface of a TiO2 Photoanode: A Rate Law Analysis. *Acs Catal.* **2017**, *7* (7), 4896–4903.

(59) Kafizas, A.; Wang, X.; Pendlebury, S. R.; Barnes, P.; Ling, M.; Sotelo-Vazquez, C.; Quesada-Cabrera, R.; Li, C.; Parkin, I. P.; Durrant, J. R. Where Do Photogenerated Holes Go in Anatase: Rutile TiO2? A Transient Absorption Spectroscopy Study of Charge Transfer and Lifetime. *J. Phys. Chem. A* **2016**, *120* (5), 715–723.

Table of Contents Figure

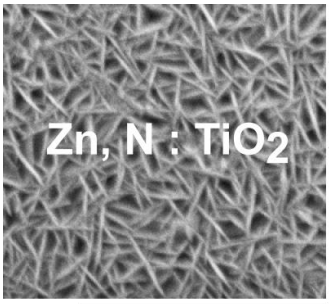
Zn, N : TiO2

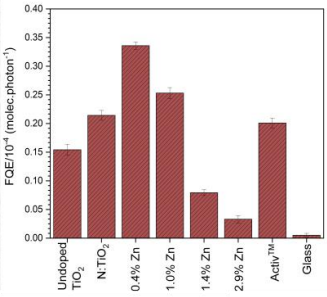
FQE/10-4 (molec.photon-1)
0.40
0.35
0.30
0.25
0.20
0.15
0.10
0.05
0.00
Undoped TiO2
N:TiO2
0.4% Zn
1.0% Zn
1.4% Zn
2.9% Zn
Activ™
Glass

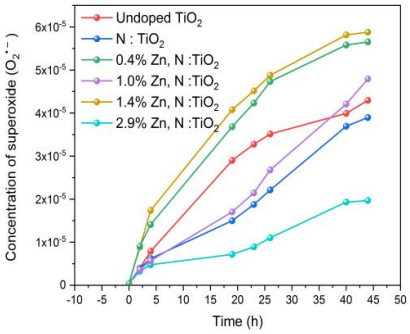
Undoped TiO2
N : TiO2
0.4% Zn, N :TiO2
1.0% Zn, N :TiO2
1.4% Zn, N :TiO2
2.9% Zn, N :TiO2
Concentration of superoxide (O2•−)
6x10-5
5x10-5
4x10-5
3x10-5
2x10-5
1x10-5
0
-10 -5 0 5 10 15 20 25 30 35 40 45 50
Time (h)